Case Studies in Thermal Engineering 32 (2022) 101889

Contents lists available at ScienceDirect

Case Studies in Thermal Engineering

journal homepage: www.elsevier.com/locate/csite

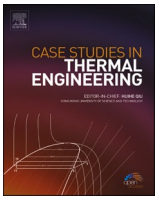

Linear thermal expansion behavior of compacted bentonite buffer materials

Seok Yoon [a], Gi-Jun Lee [a], Gyu-Hyun Go [b,*]

[a] Division of Radioactive Waste Disposal Research, KAERI, Daejeon, 34057, South Korea
[b] Department of Civil Engineering, Kumoh National Institute of Technology, Gumi, 39177, South Korea

ARTICLE INFO

Keywords:
Compacted bentonite buffer materials
Linear thermal expansion coefficient
Dilatometer test
Numerical analysis

ABSTRACT

In a geological repository system, buffer is indispensable to ensure the safe disposal of high-level radioactive waste (HLW). Because heat generated from spent nuclear fuel in a canister is released to the surrounding buffers, thermal properties of such materials are fundamental in determining the overall disposal safety. Specifically, given that thermal expansion causes thermal stress to canisters and intact rock masses in the near-field location, it is imperative to evaluate the thermal expansion characteristics of the buffer, particularly when bentonite is used. This study investigates the linear thermal expansion properties of Kyeongju bentonite buffer, a type of Ca-bentonite produced in South Korea. The linear thermal expansion coefficient of dried bentonite was measured considering the heating rate, dry density, and temperature variation using dilatometer equipment. The linear thermal expansion coefficient values of the KJ bentonite buffers were found to be 4.0–6.2 $\times$ 10^{-6}/°C. Based on test results, a numerical analysis was conducted, and the thermal strain values were similar between the test and numerical analysis. The overall linear thermal expansion coefficient of the KJ bentonite, considering radially confined or unconfined conditions and dried or saturated states, was predicted to be between 3.2 $\times$ 10^{-6}/°C and 1.0 $\times$ 10^{-5}/°C.

1. Introduction

Spent fuel from nuclear power plants releases decay heat and harmful radiation, causing frequent issues of high-level radioactive waste (HLW) disposal. Among the various types of disposal systems, deep geological repositories (where HLWs are safely isolated by a surrounding buffer), backfill, and near-field rock are preferred based on the concept of EBS (Fig. 1) in most countries because of their safety and reliability [1–4]. The buffer, an essential component of a repository, minimizes groundwater inflow from intact rock and protects the canister from any mechanical impact by filling the void between the near-field rock and the canister. Canisters packed with spent fuel are sealed with buffer and gap materials. Therefore, the hydraulic conductivity of buffers must be low to minimize the inflow of water from surrounding rocks that are saturated with groundwater [5–7]. Buffers must also have high thermal conductivity to release as much decay heat as possible from the spent fuel, as the high thermal conductivity of the buffer plays a critical role in dissipating the decayed heat [8,9].

Several studies have attempted to determine the most suitable candidate buffer materials to satisfy the requirements of the functional criteria of such a material. The results indicate that bentonite clay is among the most suitable materials [11,12]. Bentonite

* Corresponding author.
E-mail address: gyuhyungo@kumoh.ac.kr (G.-H. Go).

https://doi.org/10.1016/j.csite.2022.101889
Received 26 August 2021; Received in revised form 3 February 2022; Accepted 19 February 2022
Available online 21 February 2022

clay belongs to the smectite group, which contains large amounts of expansive montmorillonite and forms 2:1 layer platy structures that consist of two silica tetrahedral layers and an aluminum hydroxide octahedral layer [13]. Anions generated via isomorphous substitution in montmorillonite absorb cations (e.g., Na^{+}, Mg^{2+}, Ca^{2+}) between the layers to become electrostatically neutral [7]. Bentonite may be classified into Na and Ca types, depending on the exchangeable cations necessary to become neutral. In Korea, Ca-type bentonite (KJ) has been produced in the Kyeongju region by Clariant Korea and may be considered a candidate buffer material for use in the HLW repository facilities of Korea [1,9,14].

Despite various studies on the complex thermal-hydro-mechanical (THM) behaviors of bentonite buffer materials, there remains a lack of research on the thermal expansion characteristics, which is a mechanical property, in contrast to thermal properties such as the thermal conductivity and specific heat capacity. Initially, the buffers were dried from the thermal energy by the canister but reached a saturated condition from the groundwater inflow. Consequently, buffers may be subject to thermal stress due to the high-temperature heat from the canister and swelling pressure from the surrounding rock mass groundwater flow.

Research on the thermal expansion of buffers considering both dried and saturated conditions thus becomes as necessary as the study of other physical properties. In most cases, thermal expansion coefficient values have been fitted from laboratory tests by considering axial thermal strains under heating at almost saturated conditions [15–17] or determined by model calibration [18]. However, the thermal expansion characteristics under dry conditions have rarely been studied. This study investigates the thermal expansion characteristics of bentonite buffer materials under both saturated and dry conditions. The linear thermal expansion coefficient calculated according to the heating rate, dry density, and temperature range was first measured for the KJ-dried bentonite using dilatometer equipment. The thermal expansion behavior of each influencing factor was then analyzed and compared with values from other bentonites. Numerical analyses were conducted to evaluate the strain induced by thermal expansion and to compare the linear thermal expansion coefficients of both dried and fully saturated KJ bentonite specimens.

2. Dilatometer test

2.1. Test materials

The Ca-type bentonite produced in Kyeongju (KJ) contains montmorillonite (62%), albite (20%), and small amounts of quartz (5%). Table 1 presents the results of a quantitative analysis of Ca-type bentonite, based on the XRD technique, with three quantitative analyses conducted in total. Unlike the Ca-type bentonite used in this study, the amount of montmorillonite is remarkably high in MX80, a very popular commercial Na-type bentonite produced in Wyoming, USA [8,19,20]. MX80 contains montmorillonite (75%–90%), quartz (15%), and feldspar (10%) [15], and FEBEX contains more than 90% montmorillonite [19]. Table 2 shows the clay properties considering the Atterberg limits [13,21]; most bentonites are classified as CH with very high levels of plasticity based on the unified soil classification system (USCS). Higher Atterberg limits imply that they have many expansive characteristics [22]. The KJ powder was compacted into a homogeneous cylindrical specimen using cold isostatic pressing (CIP). The specimens with diameters of

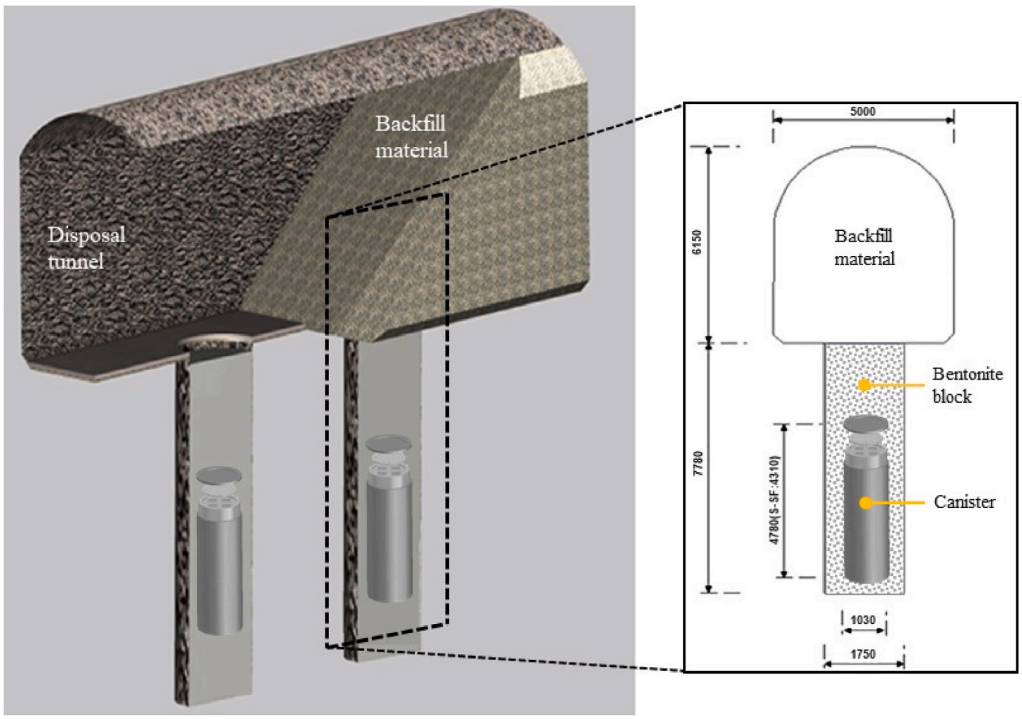

Fig. 1. Diagram of EBS (modified from Ref. [10]).

Table 1
Quantitative XRD analysis of KJ [9].

Bentonite Type	KJ powder			
Sample No.	1	2	3	Avg.
Montmorillonite	63.4	61.7	60.5	61.9
Albite	19.4	22.8	20.4	20.9
Quartz	5.8	4.9	5.3	5.3
Cristobalite	4.0	4.5	3.7	4.1
Calcite	4.3	3.3	6.8	4.8
Heulandite	3.0	2.7	3.3	3.0

Table 2
Geotechnical properties of various kinds of bentonites.

	Specific Gravity	Liquid Limit (%)	Plastic Limit (%)	Plastic Index (%)	USCS
KJ [9]	2.71	146.7	28.4	118.3	CH
MX80 [19]	2.82	350–570	70	280–500	CH
FEBEX [19]	2.7	102	53	49	MH
GMZ01 [16]	2.66	313	38	275	CH
Kunigel [31]	2.7	416	21	395	CH

10 cm and heights of 20 cm were fabricated by a cutting machine in an initial unsaturated state and fully dried for the dilatometer test.

2.2. Test equipment

Dilatometer equipment (C-Therm Technologies Ltd.) was used to measure the linear thermal expansion coefficient of the compacted bentonite buffer materials (Fig. 2). This equipment is largely composed of a furnace, chiller, and control system. The furnace creates a temperature environment for the sample, which is in contact with a pushrod. Once the sample expands owing to heat, the displacement of the pushrod is measured by a linear variable differential transformer (LVDT) sensor, which is located in the opposite position. The linear thermal expansion coefficient α_T can be obtained using Eq. (1).

$$\alpha_T = \frac{1}{L_o}\frac{\Delta L}{\Delta T} = \frac{1}{L_o}\frac{(L_i - L_o)}{(T_i - T_o)} \tag{1}$$

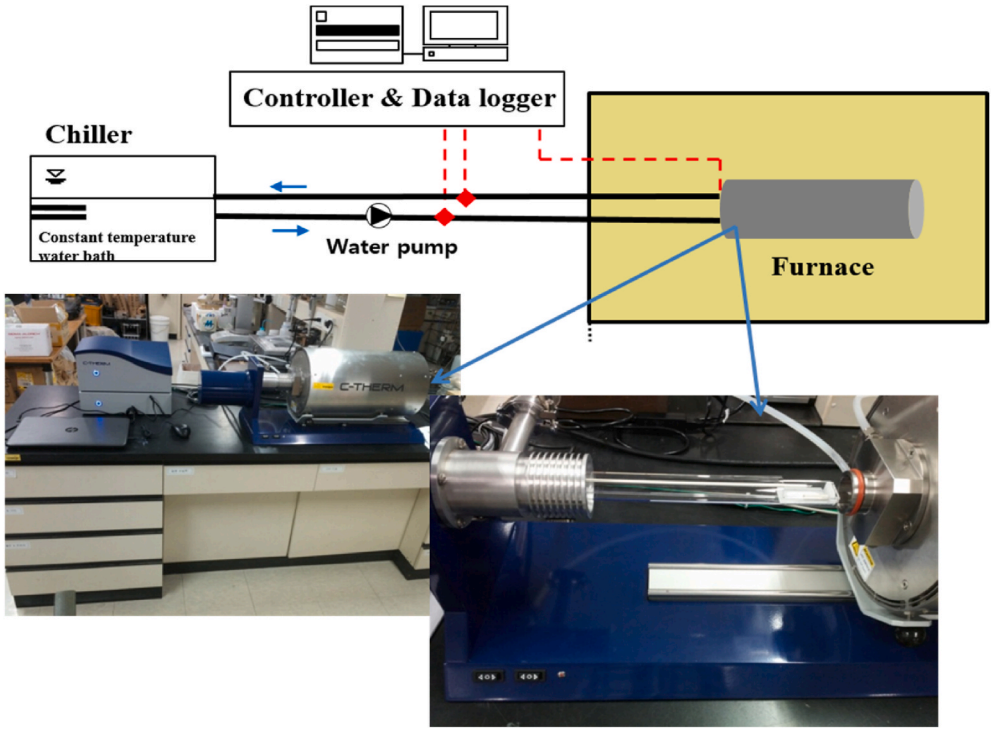

Fig. 2. Dilatometer for the measurement of the thermal expansion coefficient.

Here, α_T represents the linear thermal expansion coefficient (1/K), L is the length of the sample (mm), and T is the temperature (K). The linear thermal expansion coefficient can be determined by dividing the initial length by the length displacement at two temperature points [23].

3. Numerical simulation

In this study, numerical analyses using COMSOL Multiphysics 5.6 [24] were conducted to simulate the dilatometer test. The model evaluates the strain induced by thermal expansion and calculates the effective linear thermal expansion coefficient for both dried and fully saturated KJ bentonite specimens. During the temperature rise in the dilatometer test, the study assumed that heat propagates only by conduction in the specimen, and the heat from the phase changes of porewater due to evaporation for the saturated specimen was neglected. Thus, the energy balance equation is as follows:

$$\rho C\frac{\partial T}{\partial t}-\nabla\cdot(\lambda\nabla T)+(1-n)\beta T\frac{\partial \varepsilon}{\partial t}=0 \tag{2}$$

$$\lambda=-1.211+2.648\frac{nS}{(1-n)Gs}+1.054\rho_d+0.034\ln(T) \tag{3}$$

where ρ is the density (kg/m^3), C is the volumetric heat capacity (J/m^3/K), T is the temperature (K), *and* n is the porosity. The effective thermal conductivity, λ, depends on the dry density, saturation, and temperature, and is calculated using an empirical model [25]. β is the thermal stress parameter. ε is the volumetric strain, which is defined as the sum of the elastic strain ε_{el} and thermal strain ε_{th}. It was assumed that heat from the furnace was introduced on the surface of the bentonite specimen. The boundary condition at the surface of the specimen is as follows:

$$-\nabla\cdot(\lambda\nabla T)|_{surface}=h(T_{ext}-T) \tag{4}$$

where h is the heat transfer coefficient (W/(m^2•K)). T_{ext} is the external temperature of the specimen (K) and is applied as a function of time that matches the heating rate considered in the test.

For the mechanical analysis, it was assumed that the swelling effect due to the porewater for the saturated specimen is negligible and that the expansion is caused only by the thermal effect. The linear-elastic constitutive model with a thermal expansion term is applied as follows:

$$\rho\frac{\partial^2 u}{\partial t^2}=\nabla\cdot(C:\varepsilon_{el}) \tag{5}$$

$$\varepsilon_{elatic}=\varepsilon-\varepsilon_{th} \tag{6}$$

$$\varepsilon_{th}=\alpha_T(T)\cdot(T-T_{ref}) \tag{7}$$

$$\varepsilon=\frac{1}{2}[(\nabla u)^T+\nabla u] \tag{8}$$

where u is the displacement (m) and C is the constitutive tensor, which is a function of Young's modulus E and Poisson's ratio ν. $\alpha_T(T)$ is the thermal expansion coefficient (1/K). Bentonite consists of three different phases. The volumetric fraction, θ, of the saturated bentonite can be expressed as a function of the degree of saturation, S, and porosity, n. The material properties used in the simulation model are listed in Table 3. Here, the effective thermal expansion coefficient was assumed to follow a logarithmic law; $\alpha_{T,solid}$, $\alpha_{T,water}$, $\alpha_{T,air}$ is the thermal expansion coefficient of particle, water, and air, respectively. It can be measured through experiments under a specific dry unit weight condition. In this study, the thermal expansion coefficient of the solid particle ($\alpha_{T,solid}$) was obtained through back-calculation from the numerical simulation model by matching with the effective thermal expansion coefficient derived from the experiment under a specific dry unit weight condition. Besides, the volume fractions depend on temperature, the considered thermal expansion coefficient also varies according to the temperature increase through the coupling analysis.

Table 3
Input properties used for the simulation model.

Properties	value
Thermal expansion coefficient of solid particle (1/K)	1.24E-7
Thermal expansion coefficient of air (1/K), averaged from 30 to 105 °C	2.94E-3
Thermal expansion coefficient of water (1/K), averaged from 30 to 105 °C	5.19E-4
Convective heat transfer coefficient (W/(m^2·K))	10
Heat capacity (J·kg^{-1}·K^{-1})	660
Initial temperature (°C)	30
Young's modulus (GPa)	1.45
Poisson's ratio	0.216
Elapsed time (min)	78

$$\theta_{solid} = 1 - n, \theta_{water} = Sn, \theta_{air} = (1 - S)n \quad (9)$$

4. Results and discussion

4.1. Experimental results

In deep disposal systems, bentonite buffers are known to have low heating rates. The initial maximum heating rate at the interface between the canister and the buffer was found to be in the range of 0.1–0.3 °C/min [26], and the thermal expansion behavior of bentonite as a buffer considering the temperature increase was studied. The compacted bentonite specimens were dried at 110 °C for 48 h. In this study, dried specimens were used to investigate only the thermal expansion behavior more easily by considering various factors.

First, the thermal expansion behavior from 30 °C to 105 °C was observed from the dilatometer test with varying dry densities of the compacted bentonite. The change in the lengths of the compacted bentonite buffer materials was measured at a heating rate of 0.5 °C/min, which is the minimum heating rate of the dilatometer. As shown in Fig. 3, the length increased linearly in the temperature range of 30–105 °C, and the linear thermal expansion coefficient for the given temperature range was calculated using Eq. (1).

In addition, this study measured the linear thermal expansion coefficient for various heating rates. Although the heating rate of the buffer should be 0.1–0.3 °C/min when considering actual deep disposal systems, the heating rate was set to 0.5–10 °C/min due to the limitations of the equipment used in the experiment. As illustrated in Fig. 4, the linear thermal expansion coefficient of the bentonite buffer materials tended to decrease as the heating rate increased, with the exception of heating rates lower than 1 °C/min, which resulted in a nearly constant value of the linear thermal expansion coefficient. This is a result of the nature of bentonite as a three-phase material containing water, air, and soil particles [27]. Unlike metals, where heat is transferred across the entire specimen with a high heating rate, heat cannot be transferred properly across the entire body of bentonite because of the low thermal conductivity of water and air, resulting in temperature increases only in certain sections. As a result, the overall linear thermal expansion coefficient is lower. Therefore, setting the heating rate to 0.5–1 °C/min should not be problematic when considering actual disposal environments. The linear thermal expansion coefficient of the compacted bentonite buffer materials according to dry density was measured at heating rates between 0.5 °C and 1 °C/min, and the overall linear thermal expansion coefficient value of the dried KJ-compacted bentonites was 4.0–6.2 $\times$ 10^{-6}/°C.

4.2. Numerical simulation results

Fig. 5 shows the simulation results of the dilatometer test with radially unconfined condition. During the test, the distributions of the temperature and thermal stress were evaluated using the simulation model. Because the high-temperature distribution was relatively more concentrated on both ends of the specimen, the thermal stress was also concentrated in the tip regions (Fig. 5(a)–(b)). During the whole test, the thermal expansion coefficient calculated at each time step varies with increasing temperature, even though the difference is not very large (Fig. 5(c)). Thus, the displacement at the tip of the specimen increased almost linearly as the temperature increased (Fig. 5(d)). To verify the accuracy of the simulation model, the thermal strains at the tip of the specimen were compared between the dilatometer test and numerical model. As shown in Fig. 6, the thermal strain from the model almost matched that of the dilatometer test. Therefore, the simulation model provides a reasonable prediction for determining the thermal expansion coefficient of the compacted bentonite buffer. The linear thermal expansion coefficient was subsequently evaluated according to the initial dry density. As shown in Fig. 7, the measured and predicted linear thermal expansion coefficients decrease as the initial dry density of the bentonite buffer increases. That is, the linear thermal expansion coefficient tended to be inversely proportional to the initial dry density for both, the dilatometer test and simulation. This was because soil samples with lower dry density levels had a greater ratio of air. Since air has a thermal expansion coefficient of 2.6–3.3 $\times$ 10^{-3} (1/K), which is substantially greater than that of soil

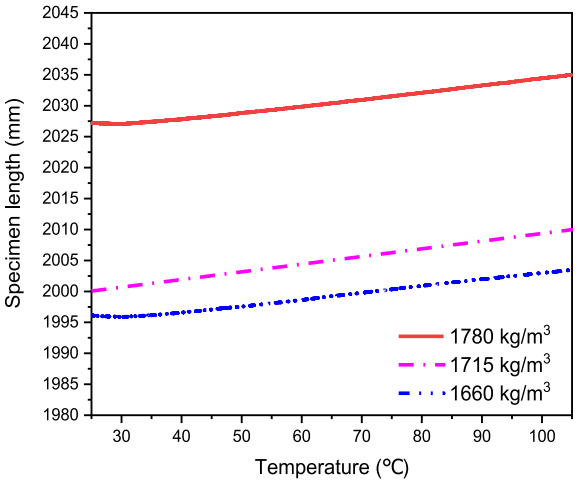

Fig. 3. Displacement with respect to the temperature range.

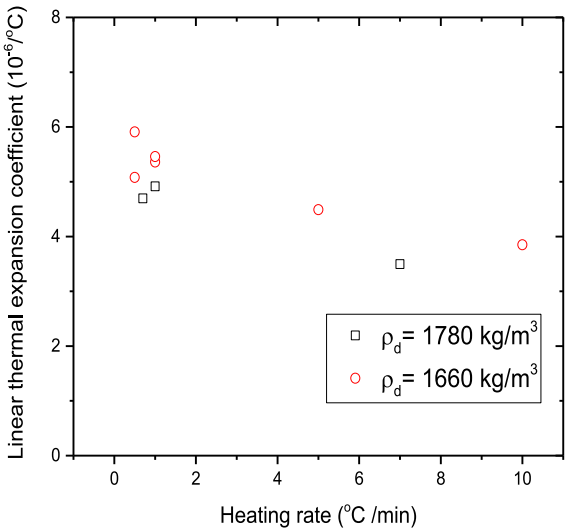

Fig. 4. Linear thermal expansion coefficient with respect to the heating rate (Dilatometer test results).

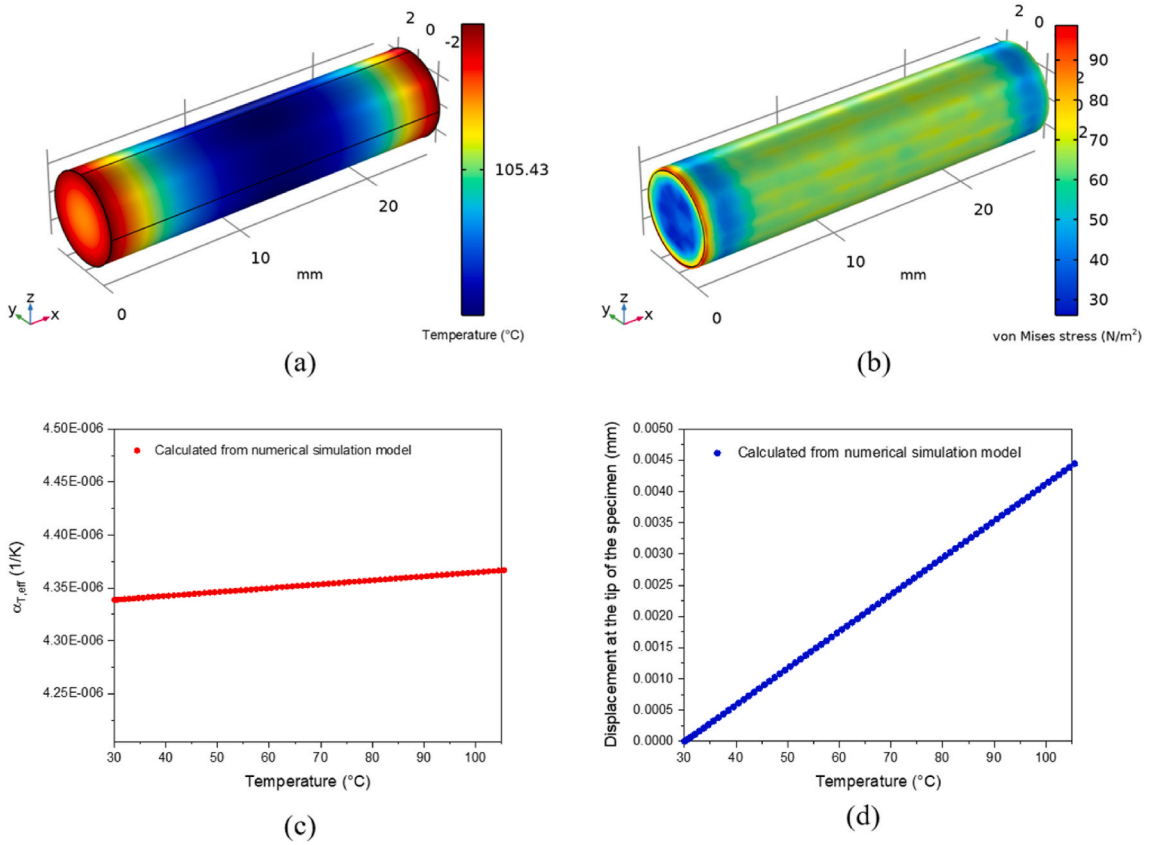

Fig. 5. Simulation result of dilatometer test: (a) Temperature distribution (after 78 min), (b) Thermal stress distribution (after 78 min), (c) Calculated effective thermal expansion coefficient, (d) Displacement due to the thermal load.

particles, this contributes to the large linear thermal expansion coefficient of the sample.

In the current status, the experimental setup using the dilatometer test has difficulty in measuring linear thermal expansion for the saturated specimen condition due to technological limitations. Thus, this study attempted to obtain the linear thermal expansion coefficient for the saturated specimen using a validated numerical simulation model. It also analyzed the thermal strain behaviors

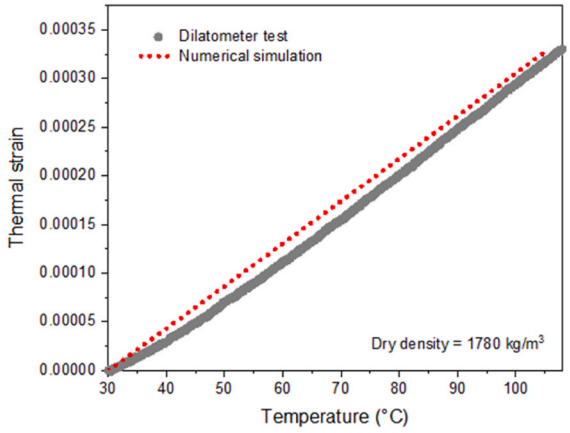

Fig. 6. Thermal strain with respect to the temperature range.

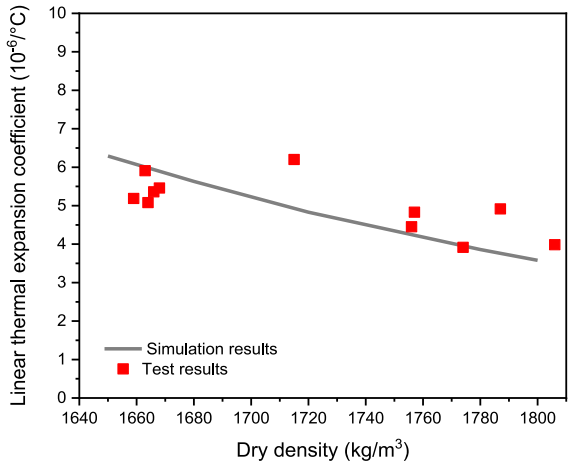

Fig. 7. Linear thermal expansion coefficient with respect to the dry density.

between radially confined and unconfined conditions based on numerical simulations. Some previous studies derived thermal expansion coefficient value from the radially confined condition [16,17]. Fig. 8 shows the comparison results of the linear thermal expansion coefficient between the dried and saturated specimen conditions from the numerical simulation model. Because the thermal expansion coefficient of water is substantially lower than that of air [28], this resulted in a relatively low linear thermal expansion coefficient value. It can also be noted that there have been larger axial thermal strain values under the radially confined condition than under the unconfined condition. It is thought that thermal expansion behavior occurs in one dimension under radial confined conditions and causes higher thermal strain. The thermal expansion coefficient values of KJ were experimentally obtained under the radially unconfined condition, which might cause relatively smaller thermal expansion coefficient values than other bentonites. The overall range of the linear thermal expansion coefficient values of KJ bentonites was derived from 3.2×10^{-6}/°C to 1.0×10^{-5}/°C, depending on the experimental conditions for the dried and saturated specimens (Table 4). Previous studies have mentioned thermal expansion coefficient values for various compacted bentonites (Table 4). MX-80 has linear thermal expansion coefficients of 2.0×10^{-4}/°C [8] and 1.0×10^{-5}/°C [15]. The linear thermal expansion coefficient of FEBEX showed 7.0×10^{-5}/°C [29] and 1.5×10^{-4}/°C [17,30]. GMZ bentonite, which contains more than 75% montrillonite, showed a linear thermal expansion coefficient of 1.0×10^{-4}/°C [16]. Rutqvist et al. [17] also derived a linear thermal expansion coefficient of 1.0×10^{-6}/°C for compacted bentonite based on model calibration with in-situ test results. The bentonite in-situ test (Kamaishi mine heater test) is Kunigel bentonite, which contains less than 50% montrillonite [31]. There have been insufficient test results to obtain thermal expansion coefficient values, and most of the results are values at a certain dry density. It showed several time differences depending on the methods used to derive the linear thermal expansion coefficient despite the same bentonite. The linear thermal expansion coefficient of KJ bentonite was 3–10 times higher than that of Kunigel, and 1.0–62 times lower than that of MX-80, FEBEX, and GMZ bentonites. It is thought that the test method may produce different results because the thermal expansion coefficient values of other bentonites were fitted from oedometer test results, which are horizontally confined conditions [16,32].

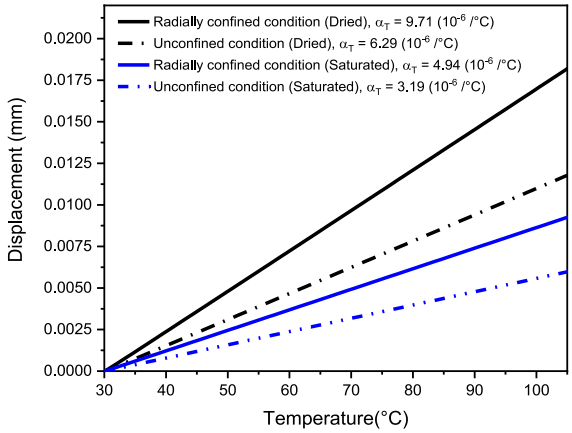

Fig. 8. Simulation results according to test conditions.

Table 4
Linear thermal expansion coefficient of various bentonites.

Bentonite Type	Linear thermal expansion coefficient (1/°C)	Methods	Ref.
KJ	3.2×10^{-6}–1.0×10^{-5} (γ_d =1.65–1.8 g/cm^3)	Dilatometer test & Numerical modeling	This study
MX-80	2.0×10^{-4} (γ_d =1.78 g/cm^3)	Isotropic cell test	[8]
	1.0×10^{-5} (γ_d =1.53 g/cm^3)	Not specified	[15]
FEBEX	7.0×10^{-5} (γ_d =1.70 g/cm^3)	Fitted parameter from Oedometer	[29]
	1.5×10^{-4} (γ_d =1.60 g/cm^3)	Fitted parameter from Oedometer	[17]
GMZ	1.0×10^{-4} (γ_d =1.69 g/cm^3)	Fitted parameter from Oedometer	[16]
Kunigel	1.0×10^{-6} (γ_d =1.65 g/cm^3)	Model calibration from in-situ test	[18]

5. Conclusion

This study adopted experimental and numerical methods to evaluate the thermal expansion properties of compacted bentonites under test conditions and dried or saturated states. The following conclusions were drawn:

First, after drying KJ-compacted bentonites, which were obtained from the Kyeongju region in Korea, the linear thermal expansion coefficients using dilatometer equipment were measured according to the heating rate and dry density at temperatures ranging from room temperature to 110 °C. As the heating rate increased, the linear thermal expansion coefficient decreased, but no significant change was observed at rates lower than 1 °C/min. Therefore, the heating rate can be set to 0.5–1 °C/min. In addition, the linear thermal expansion coefficients of compacted bentonites with various dry densities were measured, and the results showed that the linear thermal expansion coefficient decreased as the dry density increased. The overall linear thermal expansion coefficient of the dried KJ-compacted bentonites used in the test was found to be in the range of 4.0–6.0 $\times$ 10^{-6}/°C when the dry densities were 1.65–1.8 g/cm^3.

Second, the dilatometer test results were numerically simulated. The thermal strain for the dried compacted bentonites between the test and numerical simulation were similar. As it is difficult to measure the thermal strain for saturated compacted bentonite, a numerical analysis was also conducted to predict the linear thermal expansion coefficient for the saturated condition. The thermal expansion coefficients of the dried compacted bentonites were slightly higher than those of the saturated specimens. The linear thermal expansion coefficients under the radially confined condition were also higher than those under the radially unconfined condition. The overall thermal expansion coefficients of the KJ-compacted bentonites based on the dilatometer test and numerical analysis were between 3.2×10^{-6}/°C-1.0×10^{-5}/°C and derived to be several to tens of times smaller than those of MX-80, FEBEX, and GMZ bentonites. On the other hand, the thermal expansion coefficients of KJ bentonites were several times larger than those of Kunigel bentonite. Several factors, such as the test method, dry or saturated status, confined condition, and expansion characteristics of each bentonite may yield different thermal expansion behaviors. As the thermal expansion coefficients were reported differently in spite of the same types of bentonites, it is expected that the method suggested by this research may be applied efficiently to derive the thermal expansion coefficient of the compacted bentonites considering various repository conditions.

CRediT authorship contribution statement

Seok Yoon: Writing & Experiment & Editing. **Gi-Jun Lee:** Methodology, Experiment. **Gyu-Hyun Go:** Investigation, Formal analysis, Writing – review & editing.

Declaration of competing interest

The authors declare that they have no known competing financial interests or personal relationships that could have appeared to influence the work reported in this paper.

Acknowledgement

This research was supported by the Nuclear Research and Development Program of the National Research Foundation of Korea (2021M2E3A2041351), and Institute for Korea Spent Nuclear Fuel and National Research Foundation of Korea (2021M2E1A1085193).

Appendix A. Supplementary data

Supplementary data related to this article can be found at https://doi.org/10.1016/j.csite.2022.101889.

References

[1] W.J. Cho, J.W. Lee, S. Kwon, An empirical model for the thermal conductivity of compacted bentonite and a bentonite-sand mixture, Heat Mass Tran. 47 (2011) 1385–1393, https://doi.org/10.1007/s00231-011-0800-1.
[2] D.A. Dixon, M.N. Gray, A.W. Thomas, A study of the compaction properties of potential clay-sand buffer mixtures for use in nuclear fuel waste disposal, Eng. Geol. 21 (1985) 247–255, https://doi.org/10.1016/0013-7952(85)90015-8.
[3] J. Jeong, Y.M. Lee, J.W. Kim, D.K. Cho, N.Y. Ko, M.H. Baik, Progress of the long-term safety assessment of a reference disposal system for high level wastes in Korea, Prog. Nucl. Energy 90 (2016) 37–45, https://doi.org/10.1016/j.pnucene.2016.02.020.
[4] R. Přikryl, Z. Weishauptová, Hierarchical porosity of bentonite-based buffer and its modification due to increased temperature and hydration, Appl. Clay Sci. 47 (2010) 163–170, https://doi.org/10.1016/j.clay.2009.10.005.
[5] E. Castellanos, M.V. Villar, E. Romero, A. Lloret, A. Gens, Chemical impact on the hydro-mechanical behavior of high-density FEBEX bentonite, Phys. Chem. Earth 33 (2008) S516–S526, https://doi.org/10.1016/j.pce.2008.10.056.
[6] V.R. Ouhadi, R.N. Yong, A.R. Goodarzi, M. Safari-Zanjani, Effect of temperature on the re-structuring of the microstructure and geo-environmental behavior of smectite, Appl. Clay Sci. 47 (2010) 2–9, https://doi.org/10.1016/j.clay.2008.08.008.
[7] Y. MalGoBalGaeBitNaLa, C. Heui-ju, L. Min-soo, L. Seung-yeop, Measurement of properties of domestic bentonite for a buffer of an HLW Repository, J. Nucl. Fuel Cycle Waste Technol. 14 (2016) 135–147, https://doi.org/10.7733/jnfcwt.2016.14.2.135.
[8] A.-M. Tang, Y.-J. Cui, N. Barnel, Thermo-mechanical behaviour of a compacted swelling clay, Geotechnique 58 (2008) 45–54, https://doi.org/10.1680/geot.2008.58.1.45.
[9] S. Yoon, W. Cho, C. Lee, G.Y. Kim, Thermal conductivity of Korean compacted bentonite buffer materials for a nuclear waste repository, Energies 11 (2018) 2269, https://doi.org/10.3390/en11092269.
[10] J. Lee, H. Kim, I. Kim, H. Choi, D.K. Cho, Analyses on thermal stability and structural integrity of the improved disposal systems for spent nuclear fuels in Korea, J. Nucl. Fuel Cycle Waste Technol. 18 (2020) 21–36, https://doi.org/10.7733/jnfcwt.2020.18.S.21.
[11] C. Ould-Lahoucine, H. Sakashita, T. Kumada, Measurement of thermal conductivity of buffer materials and evaluation of existing correlations predicting it, Nucl. Eng. Des. 216 (2002) 1–11, https://doi.org/10.1016/S0029-5493(02)00033-X.
[12] M.V. Villar, A. Lloret, Influence of temperature on the hydro-mechanical behavior of a compacted bentonite, Appl. Clay Sci. 26 (2004) 337–350, https://doi.org/10.1016/j.clay.2003.12.026.
[13] T.W. Lambe, R.V. Whitman, Soil Mechanics, John Wiley & Sons, Inc, 1969.
[14] J.O. Lee, H.J. Choi, J.Y. Lee, Thermal conductivity of compacted bentonite as a buffer material for a high-level radioactive waste repository, Ann. Nucl. Energy 94 (2016) 848–855, https://doi.org/10.1016/j.anucene.2016.04.053.
[15] E. Ballarini, B. Graupner, S. Bauer, Thermal-hydraulic-mechanical behavior of bentonite and sand-bentonite materials as seal for a nuclear waste repository: numerical simulation of column experiments, Appl. Clay Sci. 135 (2017) 289–299, https://doi.org/10.1016/j.clay.2016.10.007.
[16] W.M. Ye, Y.W. Zhang, B. Chen, Z.J. Zheng, Y.G. Chen, Y.J. Cui, Investigation on compression behavior of highly compacted GMZ01 bentonite with suction and temperature control, Nucl. Eng. Des. 252 (2012) 11–18, https://doi.org/10.1016/j.nucengdes.2012.06.037.
[17] A. Gens, L.Do Sánchez, N. Guimarães, E.E. Alonso, A. Lloret, S. Olivella, M.V. Villar, F. Huertas, A full-scale in situ heating test for high-level nuclear waste disposal: observation, analysis and interpretation, Geotechnique 59 (4) (2009) 377–399.
[18] J. Rutqvist, L. Börgesson, M. Chijimatsu, T.S. Nguyen, L. Jing, J. Noorishad, C.-F. Tsang, Coupled thermo-hydro-mechanical analysis of a heater test in fractured rock and bentonite at Kamaishi Mine — comparison of field results to predictions of four finite element codes, Int. J. Rock Mech. Min. Sci. 38 (2001) 129–142, https://doi.org/10.1016/S1365-1609(00)00069-1.
[19] M.V. Villar, Thermo-hydromechanical characterization and process in the clay barrier of a high level radioactive waste repository. State of the Art Report, Inf. Techn. Ciemat. 1044 (2004).
[20] F.T. Madsen, Clay mineralogical investigations related to nuclear waste disposal, Clay Miner. 33 (1998) 109–129.
[21] F.A. Andrade, H.A. Al-Qureshi, D. Hotza, Measuring the plasticity of clays: a review, Appl. Clay Sci. 51 (2011) 1–7, https://doi.org/10.1016/j.clay.2010.10.028.
[22] J. Atkinson, in: The Mechanics of Soils and Foundations, second ed., CRC Press, 2007.
[23] ASTM E228-17, Standard Test Method for Linear Thermal Expansion of Solid Materials with a Push-Rod Dilatometer, 2017.
[24] COMSOL Inc, Introduction to Comsol Multiphysics, Comsol, Inc., USA, 2020.
[25] S. Yoon, M.J. Kim, S. Park, G. Kim, Thermal conductivity prediction model for compacted bentonites considering temperature variations, Nucl. Eng. Technol. 53 (2021) 3359–3366, https://doi.org/10.1016/j.net.2021.05.001.
[26] M.J. Kim, S.R. Lee, J.S. Jeon, S. Yoon, Sensitivity analysis of bentonite buffer peak temperature in a high-level waste repository, Ann. Nucl. Energy 123 (2019) 190–199, https://doi.org/10.1016/j.anucene.2018.09.020.
[27] N.N. Vasu, S.R. Lee, A hybrid feature selection algorithm integrating an extreme learning machine for landslide susceptibility modeling of Mt. Woomyeon, Souith Korea, Geomorphology 263 (2016) 50–70, https://doi.org/10.1016/j.geomorph.2016.03.023.
[28] Y.A. Cengel, A.J. Ghajar, in: Heat and Mass Transfer: Fundamentals and Applications, fourth ed., McGraw-Hill Education, 2011.
[29] F. Dupray, B. François, L. Laloui, Analysis of the FEBEX multi-barrier system including thermoplasticity of unsaturated bentonite, Int. J. Numer. Anal. Methods GeoMech. 37 (2013) 399–422, https://doi.org/10.1002/nag.1103.
[30] H. Xu, L. Zheng, J. Rutqvist, J. Birkholzer, Numerical study of the chemo-mechanical behavior of FEBEX bentonite in nuclear waste disposal based on the Barcelona expansive model, Comput. Geotech. 132 (2021), 103968, https://doi.org/10.1016/j.compgeo.2020.103968.
[31] JNC, Evaluation of Coupled Thermos-Hydro-Mechanical Phenomena in the Near Field for Geological Disposal of High-Level Radioactive Waste. TN8400, 2000, pp. 2000–2008.
[32] L. Börgesson, H. Hokkmark, O. Karnland, Rheological Properties of Sodium Smectite Clay, 1983. SKB Technical Report 88-30.